Metabolic adaptation of acute lymphoblastic leukemia to the central nervous system microenvironment is dependent on Stearoyl CoA desaturase

Angela Maria Savino[a,b*], Sara Isabel Fernandes[c*], Orianne Olivares[d*], Anna Zemlyansky[f], Antony Cousins[d], Elke K.Markert[d,e], Shani Barel[a,b], Ifat Geron[a,b], Liron Frishman[a,b], Yehudit Birger[b,f], Cornelia Eckert[g], Sergey Tumanov[e], Gillian MacKay[e], Jurre J. Kamphorst[e,1], Pawel Herzyk[h,i], Jonatan Fernández-García[c], Ifat Abramovich[c], Inbal Mor[c], Michela Bardini[j], Ersilia Barin[k], Sudha Janaki-Raman[l], Justin R. Cross[l], Michael G. Kharas[k], Eyal Gottlieb[c*], Shai Izraeli[a,b,f*], Christina Halsey[d*]

[a]Faculty of Medicine, Tel Aviv University, Tel Aviv, Israel; [b]Sheba Medical Center, Ramat Gan, Israel; [c]The Ruth and Bruce Rappaport Faculty of Medicine, Technion - Israel Institute of Technology, Haifa, Israel; [d]Wolfson Wohl Cancer Research Centre, Institute of Cancer Sciences, College of Medical Veterinary and Life Sciences, University of Glasgow, Glasgow, UK; [e]Cancer Research UK Beatson Institute, Glasgow, UK; [f]Schneider Children's Medical Center of Israel, Petach Tiqva, Israel; [g]Charite University, Berlin, Germany; [h]Glasgow Polyomics, College of Medical Veterinary and Life Sciences, University of Glasgow, Glasgow, UK; [i]Institute of Molecular, Cell and Systems Biology, College of Medical Veterinary and Life Sciences, University of Glasgow, Glasgow, UK; [j]Centro Ricerca Tettamanti, Fondazione MBBM, Universita degli Studi di Milano-Bicocca, Monza, Italy; [k]Molecular Pharmacology Program, Center for Cell Engineering, Center for Stem Cell Biology, Center for experimental Therapeutics, Center for Hematologic malignancies, Memorial Sloan Kettering Cancer Center, New York, NY, USA; [l]Donald B. and Catherine C. Marron Cancer Metabolism Center, Sloan Kettering Institute, Memorial Sloan Kettering Cancer Center, New York, NY, USA.

[1]Current address: Rheos Medicines, Cambridge Massachusetts
*Share equal contribution to this work

Corresponding authors: Christina Halsey: chris.halsey@glasgow.ac.uk, tel: +44(0)141 330 8135; Shai Izraeli: sizraeli@gmail.com, tel +972(0)526666360; Eyal Gottlieb: e.gottlieb@technion.ac.il, tel +972(0)48295469

Key words: metabolic reprogramming, acute lymphoblastic leukemia, central nervous system, SCD1, fatty acid synthesis

Competing interests: E.G. is a Board member and a Shareholder of Metabomed Ltd Israel, J.J.K. is an employee and shareholder of Rheos Medicines Inc. All other authors declare no potential conflicts of interest.

Running title: SCD1 mediates metabolic adaptation of ALL to the CNS

ABSTRACT

Metabolic reprogramming is a key hallmark of cancer, but less is known about metabolic plasticity of the same tumor at different sites. Here, we investigated the metabolic adaptation of leukemia in two different microenvironments, the bone marrow and the central nervous system (CNS). We identified a metabolic signature of fatty-acid synthesis in CNS leukemia, highlighting Stearoyl-CoA desaturase (*SCD1*) as a key player. *In vivo* SCD1 overexpression increases CNS disease, whilst genetic or pharmacological inhibition of SCD1 decreases CNS load. Overall, we demonstrated that leukemic cells dynamically rewire metabolic pathways to suit local conditions and that targeting these adaptations can be exploited therapeutically.

INTRODUCTION

Metabolic reprogramming is acknowledged as a hallmark of cancer, encompassing the idea that cancer cells adapt their metabolism to support cell proliferation and to survive in hypoxic and or nutrient-poor environments[1–3]. In hematologic malignancies, harnessing metabolic reprogramming of cancer cells has proven to be clinically useful in diagnostics such as Positron Emission Tomography and in identification of discrete subgroups in diffuse large B-cell lymphoma requiring specific therapeutic approaches[4,5]. Metabolic vulnerabilities of hematologic malignancies can be potentially exploited therapeutically[6,7]. In fact, successes in exploiting metabolic vulnerabilities as a therapeutic approach have been most notable in acute lymphoblastic leukemia (ALL) where the use of asparaginase is a cornerstone of most modern treatment protocols,

targeting the asparagine-dependent leukemic cells[8]. Despite a recent explosion in cancer metabolism research, little is known about how metabolism dynamically changes in cancer cells in response to migration from one tissue compartment to another. Here we investigated how ALL cells metabolically-adapt to the CNS microenvironment upon migration from the bone marrow (BM) and tested whether this adaptation can inform novel targeted therapies for CNS leukemia.

ALL commonly infiltrates the CNS and successful eradication is essential for long-term remission[9]. Indeed, the largest advance in cure rates for ALL patients came with the introduction of universal CNS-directed therapy in the 1970s[10]. Although relatively effective, current CNS-directed therapy in the form of intrathecal and systemic high dose methotrexate, or less commonly craniospinal irradiation, is associated with significant neurotoxicity[11,12]. A lack of mechanistic understanding of CNS leukemia has hindered the development of targeted, less toxic, therapeutic approaches.

Early post-mortem histopathology of CNS leukemia identified that blast cells infiltrate the leptomeninges and generally stay confined within this compartment[13]. More recent work using animal models and patient-derived xenografts has identified a generic property of ALL cells that enables CNS colonization. Previous published work from our laboratory in mouse and human has established that there is no evidence of a selection for subclones within the CNS microenvironment although altered expression of certain genes, such as CCR7, can enhance the process of CNS-entry[14–19]. It is postulated that the CNS may act as a “sanctuary site” where leukemic cells are able to evade the

immune response and be less exposed to systemic chemotherapy[9,20]. Successful adaptation to the CNS niche is an essential pre-requisite for long-term survival of leukemic cells, and for subsequent disease relapse in this extramedullary site.

Within the CNS niche, ALL cells are bathed in cerebrospinal fluid (CSF) within the leptomeningeal regions which is poorly vascularized and restricted by the blood-CSF barrier and therefore poor in nutrients and oxygen[21–23]. In contrast, sites of systemic engraftment, such as spleen or bone marrow, are well vascularized and constitute a rich niche with mesenchymal cells, cytokines and chemokines, favoring leukemic cell survival and proliferation[24–26]. Since leukemic blasts need energy and metabolic building blocks to survive and proliferate, and CSF nutrient supplies are scarce, we hypothesized that changes in metabolism would take place when ALL engrafts in the CNS. Using gene expression profiles and metabolic characterizations of leukemic cells in different niches, followed by gene ablation and pharmacologic manipulation of the cells, we identified an essential role for the fatty-acid synthesis gene, stearoyl co-A desaturase (*SCD1*), in CNS localization.

RESULTS

CNS-derived ALL cells display a lipid oriented metabolic transcriptional signature

To investigate transcriptional adaptations of ALL to the CNS microenvironment two human leukemic cell lines, SEM and REH, were used. SEM cells have the t(4;11) *KMT2A-AFF1* (*MLL-AF4*) chromosomal translocation and REH cells have the t(12;21)

ETV6-RUNX1 (*TEL-AML1*) translocation, representing high-risk and standard-risk subtypes respectively. Cells were transplanted into immunodeficient mice. CNS tropism was demonstrated for both cell lines and they invaded the leptomeninges in a timeframe ranging from 4 to 5 weeks (**Supplementary Figure 1**). At experimental endpoint, blasts were retrieved from the CNS and periphery (spleen), and their gene expression profiles were compared using RNA-sequencing (experimental workflow shown in **Supplementary Figure 2A**).

The human SEM cells' gene expression profiles clustered according to site of colonization in the transplanted mice; CNS versus spleen (**Figure 1A**). Differentially expressed genes were ranked according to adjusted p-values and interestingly, genes associated with cellular metabolism or stress responses comprised 12 of the top 20 protein-coding genes (**Supplementary Figure 2B-I**). This was also the case with transplanted REH cells, where 14 of the top 20 genes where associated with metabolism or stress response (**Supplementary Figure 2B-II**), supporting our hypothesis that metabolic adaptation is a key feature of successful CNS engraftment. Further analysis using gene set enrichment algorithms (GSEA) identified positive correlation of lipid and lipoprotein metabolism signatures in CNS-derived cells, with particular propensity towards fatty acid synthesis (**Figure 1B I and III**). On the other hand, oxidative phosphorylation processes, linked to fatty acid degradation, were negatively correlated with CNS involvement and enriched in SEM cells from the spleen of transplanted mice (**Figure 1B II-III**)**.** The same pattern was observed in mice transplanted with REH cells (**Supplementary Figure 2C**).

CSF is a fatty acid-poor compartment compared to the plasma

CNS leukemic blasts are surrounded by the CSF. Since the strongest metabolic signature reported above indicated that *de novo* fatty acid and lipid synthesis is upregulated when ALL cells reach the CNS, we analyzed the fatty acid content of the CSF to understand this transcriptional adaptive response. The fatty acid content of normal CSF and plasma from both non-leukemic humans and mice was characterized by mass spectrometry (**Figure 1C-D**). In both species, fatty acids are scarce in the CSF compared to plasma. This suggests that ALL cells require to perform *de novo* synthesis of fatty acids rather than rely on exogenous supply, in order to support their survival and proliferation in the CNS. Mass spectrometric analysis of mouse CSF demonstrated that all metabolic precursors for fatty acid synthesis are present in comparable levels to those in plasma (**Table 1**), as observed in humans (**Supplementary table 1**). Furthermore, precursors for fatty acid synthesis were also present in the CSF even in the presence of leukemic infiltration (**Table 1**).

SCD1 is highly expressed in human CNS leukemic blasts

Lipid anabolism is a pivotal cellular process converting nutrients into building blocks for membrane biogenesis and for generating signaling molecules. The main lipid metabolic genes and pathways, for both fatty acid synthesis and degradation, are depicted in **Supplementary Figure 3**. To examine if upregulation of *de novo* fatty acid synthesis, was a generic adaptation to the CNS microenvironment in ALL, we expanded our

157 investigation to primary patient samples and additional ALL cell lines. Expression levels
158 of a panel of genes were measured by qPCR in blasts collected from CNS and spleen
159 of mice transplanted with 5 ALL patient-derived samples (3 with t(12;21) ALL and 2 with
160 t(4;11)) (**Figure 2A**). Further validation was obtained from an independent cohort of
161 mice transplanted with REH and SEM cells (**Supplementary Figure 4A**) and with a
162 third transplanted human cell line, 018z with known high CNS-tropism[9,27]
163 (**Supplementary Figure 4B**). Furthermore, analysis of two publicly available gene
164 expression datasets from ALL patients[14,15] confirmed a lipid biosynthetic signature in
165 CNS ALL compared with bone marrow (**Figure 2B, Supplementary Figure 5**). The first
166 dataset compared ALL cells from patients with CNS relapse to ALL cells from the bone
167 marrow at diagnosis and after relapse (GSE60926)[15].The second dataset compared
168 primary samples xenografted in mice and collected from the CNS or bone marrow
169 (GSE89710)[14]. Altogether, our results derived from cell lines and patients confirmed
170 upregulation of genes involved in fatty acid synthesis and downregulation of oxidative
171 phosphorylation genes in the CNS. In particular, *SCD1* was consistently and strongly
172 upregulated in all data sets (**Figures 2A-B and Supplementary Figures 4A-B**).
173 Furthermore, SCD1 protein levels were high in 018z and SEM cells derived from the
174 CNS compared to bone marrow derived cells (**Figure 2C and Supplementary Figure**
175 **4C**).

176

177 **Increased *SCD1* expression enhances CNS infiltration in ALL**

178 SCD1 is responsible for the generation of mono-unsaturated fatty acids via the addition
179 of a double bond in the 9th position of extracellular-derived and *de novo* synthesized

saturated fatty acyl-CoAs. This leads to sequential synthesis of different classes of fatty acids, eventually resulting in either triglyceride storage in lipid droplets or phospholipid production for biomass (**Supplementary Figure 3**). Interestingly, our analysis of the fatty acid composition of the CSF demonstrated that it is very low in fatty acids in general and extremely poor in oleic and palmitoleic acids, the main products of SCD1 (**Figure 1C-D**). Given the requirement to overcome a lipid poor microenvironment, we hypothesized that increased *SCD1* expression would provide a relative growth or survival advantage to the cells in the CNS. To test whether upregulation of *SCD1* supports CNS leukemia tropism, we overexpressed *SCD1* in leukemic cells. *SCD1* overexpression in 018z cells was confirmed by qPCR and immunoblotting (**Figure 3A-B**). Relative SCD1 activity in cells was assessed by the ratio of mono-unsaturated fatty acyl-CoAs to their saturated precursors, i.e. the ratio of oleoyl-CoA to stearoyl-CoA and the ratio of palmitoleoyl-CoA to palmitoloyl-CoA. The ratio between these mono-unsaturated to saturated fatty acyl-CoAs increased in the *SCD1* overexpressing 018z cells, confirming increased SCD1 activity (**Figure 3C I-II**). The increased ratio of unsaturated/saturated fatty acyl-CoAs in *SCD1* overexpressing cells mirrored the ratio of these fatty acids either as free fatty acids or as lipid esterified pools (**Supplementary Figure 6A-B**).

In vivo, mice transplanted with SCD1-high 018z cells demonstrated significantly increased disease burden in the CNS but not in the bone marrow or spleen at experimental endpoint (**Figure 3D**)**.** This correlated with a faster onset of CNS disease manifested by a clinical phenotype of earlier hind limb paralysis compared to controls

(day 15 in SCD1-high cells as opposed to day 18-21 in control cells – **Supplementary Video 1**). Analysis of free fatty acids ratios in the CNS-engrafted cells demonstrated increased SCD1 activity in overexpressing vs. control 018z cells (**Supplementary Figure 7A**).

SCD1 overexpression in REH cells with generally lower propensity for CNS tropism (**Supplementary Figure 7B**) also induced rapid CNS engraftment at 3 weeks, a time at which control REH cells do not invade the CNS (**Figure 3E**). Mice transplanted with SCD1-high REH cells showed the same phenotype of earlier hind limb paralysis and accumulation of leukemic cells in the CNS seen with the more naturally CNS-tropic 018z cells. Control REH transplanted mice did not show any CNS engraftment at 3 weeks. SCD-1 high REH cells also showed a less pronounced but statistically significant increase in spleen tumor load and comparable tumor load in the bone marrow (**Figure 3E**).

To directly test if high *SCD1* expression confers a competitive advantage to the formation of CNS ALL we labelled the SCD1-high 018z cells with GFP and the control 018z cells with either GFP or mCherry. While GFP expression in control cells did not provide any advantage in CNS colonization compared to control cells expressing the mCherry, the GFP-labelled SCD1-high cells showed a clear competitive advantage in the CNS but not in the periphery (**Figure 3F-G**).

SCD1 inhibition decreases CNS leukemia burden

As SCD1 controls a key step in fatty acid synthesis, we hypothesized that blocking the activity of the enzyme would impair ALL survival and/or proliferation in the lipid-deprived CNS microenvironment. CRISPR/CAS-9 technology was used to ablate *SCD1* in CNS-tropic 018z cells. Several guide RNAs were screened and gRNA4 resulted in the most pronounced decrease in SCD1 protein (**Figure 4A**) consistent with decreased mRNA transcripts (**Figure 4B**). To examine if *SCD1* affects cell growth in lipid poor environments similar to the CSF*,* we cultured the cells in media containing delipidated serum. Delipidation itself did not affect the concentration of common nutrients in the serum (**Supplementary Figure 8**). SCD1-low cells cultured in medium supplemented with the delipidated serum showed decreased proliferation compared with cells cultured in full medium, while proliferation of control cells was not affected (**Figure 4C**). A significant decrease in the oleoyl-CoA to stearoyl-CoA ratio, and palmitoleoyl-CoA/palmitoyl-CoA ratio (**Figure 4D I-II**) indicated that SCD1 enzymatic activity was indeed decreased in SCD1-low cells. The decrease in the ratio of monounsaturated fatty acyl-CoAs to their saturated precursors reflected the decreased ratios of free and lipid esterified fatty acids following *SCD1* downregulation (**Supplementary Figure 6C-D**).

Importantly, the tumor load in the CNS was significantly decreased in mice engrafted with SCD1-low cells compared to control (**Figure 4E**). This was not associated with a general decline in biological fitness of the cells as decrease in cell number was not consistent among all tissues, as indicated by an elevated engraftment of SCD1-low cells

in the bone marrow compared with the control. Clonal escape from *SCD1* downregulation in the bone marrow was excluded by measuring SCD1 protein expression in leukemic cells engrafting the bone marrow, which confirmed ongoing suppression (**Figure 4F**).

To further confirm the dependency on SCD1 under lipid deprived conditions using a pharmacologic approach, 018z cells were cultured in lipid rich or lipid deprived conditions in the presence or absence of the SCD1 inhibitor SW203668[28]. While the inhibitor caused a slight decrease in proliferation of control cells in full serum, the effect of SCD1 inhibition was more pronounced when cells were cultured in delipidated serum (**Figure 5A-D**). This decrease in cell number was mitigated in SCD1 overexpressing cells (**Figure 5A, 5C**) and as expected, SCD1 inhibition showed minimal or no effect in SCD1-low cells (**Figure 5B, 5D**)**.**

In order to explore whether SCD1 inhibitors could be a therapeutic option to prevent CNS relapse, we treated transplanted mice with the above mentioned SCD1 inhibitor. To better monitor the localization of engrafted cells, 018z cells were transduced with a lentivirus expressing the luciferase reporter gene. Following transplantation, mice were treated with SCD1 inhibitor for 10 days after which bioluminescent imaging was used to assess leukemic burden. This was followed by CNS and bone marrow blast counts as before. Both whole-body imaging and assessment of blasts in different tissue sites demonstrated a general impairment of 018z engraftment in transplanted mice (**Figure 5E**), decreasing the tumor load both in the bone marrow and CNS (**Figure 5F-G**). It

should be noted however that the decrease in disease burden was greater in the CNS (88.31% decrease) than the bone marrow (47.21% decrease).

Moreover, we extended our experiments to primary ALL samples (patient-derived xenografts – PDXs). We selected 4 PDXs with variable but overall fast and aggressive CNS phenotype (PDXs features are summarized in **Supplementary Table 2**). Treatment with SW203668 (20 mg/kg-daily) started 1 week after the transplant. The treatment was not associated with systemic toxicity as confirmed by no changes in body weight of treated mice (**Supplementary Figure 9**). At sacrifice, treated mice from all PDX groups showed a consistent reduction in CNS tumor load compared with respective vehicle control groups, though not all reached statistical significance (**Figure 6A-D**). Importantly, in all PDX models, the first mouse to reach endpoint with signs of sickness was from the vehicle treated group. In 3 of the 4 PDX groups (PDXs 1, 3, 4) there was no significant effect on BM engraftment (**Figure 6A, 6C-D**), while PDX 2 showed increased BM tumor load upon SCD1 inhibitor treatment (**Figure 6B**), similar to the effect observed in 018z SCD1-low model (**Figure 4E**). Taken together, these results confirm that CNS leukemia is sensitive to SCD1 pharmacological inhibition pointing to SCD1 inhibition as a specific therapeutic strategy.

DISCUSSION

Metabolic adaptation to environmental settings is a key hallmark of cancer, and therefore is potentially exploitable therapeutically. In this work, we used leukemic cells

residing in the bone marrow and CNS to investigate metabolic changes occurring in a single cancer in two different compartments *in vivo*. These two regions are substantially different in their nutrient availability in general and fatty acid availability in particular.

Optimal management of CNS leukemia remains a clinical challenge with current treatments producing high levels of neurotoxic side effects and lacking efficacy in a subset of patients. An understanding of the mechanism by which leukemic blasts survive in the nutrient poor CNS is an important step to designing targeted therapies with improved toxicity profiles. Work to date using preclinical models has identified that CNS entry of leukemic blasts is relatively unrestricted and that survival in this hostile environment is likely to be the key determinant of relapse risk[9,17,29]. Therefore, we investigated adaptations of leukemic blasts to the CNS niche in order to identify potential vulnerabilities.

Our transcriptional data show that leukemic adaptation to the CNS is primarily metabolic with alterations in fatty acid synthetic pathways being particularly prominent. The *SCD1* gene was identified as a consistently upregulated target in several complementary datasets. These findings are supported by the very low levels of fatty acids in CSF compared to plasma. Fatty acids are used by the cells catabolically for oxidation in order to generate energy, and anabolically, to produce triglycerides, phospholipids, and cholesterol esters, which serve as important sources of structural components and biomass. Monounsaturated fatty acids can either be taken up from the environment or produced *de novo* in a process involving SCD1. Interestingly, cancer cells under

316 hypoxic conditions tend to bypass SCD1 and preferably import fatty acids[30]. While the
317 CSF is relatively low in oxygen, it is also an extremely poor source of fatty acids, so
318 cancer cells in the CSF may have a particular dependence on *de novo* synthetic
319 pathways.

320

321 Upregulation of *SCD1* expression has been reported in primary tumors in breast[31],
322 lung[32], kidney[33], gastrointestinal tract[34] and prostate[35] as well as chronic myeloid
323 leukemia[36] and B-cell lymphoma[5,15,37]. Our findings in ALL are strongly supported by a
324 recent study investigating potential biomarkers for risk of CNS relapse[15] which identified
325 upregulated *SCD1* and osteopontin expression in bone marrow blasts of patients who
326 went on to experience a CNS relapse. Our work demonstrates a direct functional role
327 for *SCD1* in the CNS microenvironment mechanistically linked to the reduced availability
328 of fatty acids in CSF compared to plasma.

329

330 SCD1 inhibitors have been developed by the pharmaceutical industry primarily for
331 treatment of steatohepatitis and obesity. However, interest has increased recently in
332 their use as anti-cancer agents[38]. Using a systems biology approach to predict selective
333 drug targets on the basis of cancer metabolic networks, a specific dependence of
334 cancer cells on lipid metabolism enzymes was identified[39]. This model predicted that
335 targeting enzymes involved in these processes should selectively interfere with the
336 growth of cancer cells without overt toxicity towards normal tissues. There is evidence
337 of pre-clinical efficacy in a variety of tumor models, including Burkitt lymphoma and
338 acute myeloid leukemia[37]. Although previous studies have reported side effects in

mouse models[40,41], including eye mucosal dysfunction, squinting and skin barrier dysfunction, they can be considered of less clinical severity compared to the wide spectrum of severe symptoms associated with commonly used chemotherapeutic agents such as heart failure and broader systemic toxicity. Of note, we did not detect any gross toxic effects in mice treated with SW203668. Therefore, the potential benefits of SCD1 anti-cancer properties may outweigh their risk of side effect.

Another possible concern is the potential adaptive metabolic rewiring of cancer cells to circumvent metabolic inhibitors. For example, a recent study identified activation of an alternative desaturation pathway from palmitate to sapienate in response to SCD1 inhibition in hepatocellular carcinoma cells[42]. There is also evidence that activation of autophagy may act as a resistance mechanism for SCD1 inhibition in colorectal cancer cell lines[43]. This suggests that multi-drug approaches may be needed to prevent compensatory “re-wiring” in the face of metabolic inhibitors.

Importantly, several lines of evidence from other works suggested that the metabolic adaptations we observed in the CNS are not “hardwired” as genetic mutations or selection of clones with pre-existing high levels of expression[17,29]. Rather, they are reversible adaptive changes to a novel microenvironment. This of course raises the possibility that cells may also be able to escape SCD1 inhibition by moving to a new microenvironment rich in exogenous lipids. Indeed, this may explain the variable effect of SCD1 inhibition on leukemic cells in the BM (**Figure 6**). Nevertheless, the bone marrow disease burden can be dealt with using other therapeutic approaches, while the

SCD1 inhibition might be used to eliminate CNS involvement. The degree of dynamic movement in and out of the CNS by leukemic blasts is currently unknown. However, in childhood ALL, CNS relapse is rarely truly "isolated" and sub-microscopic bone marrow involvement is detected with sensitive molecular techniques in the majority of cases[44].

The concept of metabolic heterogeneity in tumors until now has mainly focused on three areas. Firstly, the influence of different tumor-initiating genetic lesions in the same primary cancer type[5,45]. Secondly, differences between solid tumors originating in different tissues e.g. lung vs. breast[45]. Thirdly, the influence of local hypoxia or differences in nutrient availability as tumors enlarge in their primary sites[46]. All of these local effects can "prime" tumors to develop drug resistance or develop capacity to metastasize to distant sites[47,48]. In this paper, we highlight a fourth area – metabolic plasticity demonstrated by cancer cells when entering a new tissue microenvironment. This has important implications for therapeutic targeting of metabolism in the setting of metastatic disease or disseminated hematological malignancies and supports the use of multi-agent therapy. Moreover, it adds a further layer of complexity to the already recognized issue of intra-tumoral genetic heterogeneity[49].

METHODS

Cell culture

REH [t(12;21) *ETV6-RUNX1 (TEL-AML1)*] and SEM [t(4;11) *KMT2A-AFF1 (MLL-AF4)*] cell lines were bought from ATCC. 018z [(47, XY, +8, del(9)(p13))], were a kind gift of

Dr. L.H. Meyer from Ulm University. 018z cells were maintained in RPMI supplemented with 20%FBS, L-glutamine 2mM, non-essential amino acids (0.1 mM glycine, L-alanine, L-asparagine, L-aspartic acid, L-glutamic acid, L-proline, L-serine) (Gibco-BRL), and sodium pyruvate 1 mM (Sigma). REH and SEM cells were maintained in Glutamax 25mM glucose Dulbecco's modified Eagle's medium (DMEM) supplemented with 10% (vol/vol) FBS (Life Technologies), 1% penicillin/streptomycin solution. Cells were cultured at 37°C at 21% oxygen in a 5% CO_2 incubator and were regularly monitored for mycoplasma contamination. Unless otherwise stated, all cell culture reagents were purchased from Thermo Fisher Scientific (Life Technologies).

***SCD1* Knockout**

CRISPR/Cas9 technology was used to knockout *SCD1*. Exon 3 of the *SCD1* gene was targeted by designing guide RNAs (gRNA) using the publicly available software tool (crispr.mit.edu:8079/). Seven top-scored gRNAs were cloned into pLentiCRISPR.EFS.GFP (Addgene plasmid #57818, a gift from Benjamin Ebert, Division of Hematology, Department of Medicine, Brigham and Women's Hospital, Harvard Medical School, Boston) according to published protocols[50]. Following cloning, plasmids were transformed into compatible stable bacteria. Single colonies were picked, and extracted plasmids were sequenced. For efficiency validation, a surveyor assay was performed using GUIDEIT validation kit (Clontech Laboratories) and the most-efficient gRNA was selected for virus production (Strand guide sequence: 5'-GGCCGAGCTTTGTAAGAGCGG-3'). 018z cells were then transduced and 3 days later

were sorted for GFP and seeded for 7 days, with media changes every 72 hours. The scramble vector (pLentiCRISPR.EFS.GFP) was used as the control vector.

Verification of Endogenous *SCD1* Gene Editing

Cells were transduced with the pLentiCRISPR.EFS.GFP construct targeting *SCD1*. Cells positive for GFP were sorted and cultured for 7 days. Genomic DNA was extracted from the sorted population and from wild type 018z cells with the QIAamp DNA Mini Kit (Quiagen), and CRISPR target regions amplified using appropriate locus-specific primers (FW: 5'-AGCCTGACGAAGACAGTTTCT-3'; REV: 5'-TGCTTTATGGACTTAAGGACTG-3'). Standard PCR conditions were used with Taq Ready mix (HyLabs) and 100 ng of genomic DNA per the manufacturer's instructions for 35 cycles. The correct size of the PCR product was checked by agarose gel electrophoresis. PCR products were then purified with Wizard SV Gel and PCR Clean-Up System Protocol (Promega) and then Sanger-sequenced. RNA was extracted from 018z cells after sorting using Direct-zol RNA MiniPrep Kit (Zymo Research) and cDNA was synthesized using qScript cDNA Synthesis Kit. CRISPR target regions amplified using appropriate locus-specific primers were sequenced and compared using TIDE software.

SCD1 overexpression

Cloning of *SCD1* gene was performed with standard cloning protocols. All fragments amplifications were carried out using Phusion High-Fidelity PCR Master Mix

(Finnzymes, Espoo, Finland) in touchdown PCR program to account for different melting temperature of primers. Amplified fragments were purified directly from PCR reaction using the Wizard SV Gel and PCR Clean-up System (Promega). Fragments and vectors were digested using restriction enzymes according to manufacturer's protocols (NEB Ipswich, MA) and purified after gel electrophoresis using the Wizard SV Gel and PCR Clean-up System (Promega). Quick ligation kit (NEB Ipswich, MA) was used to ligate the vectors and inserts. The ligations were transformed to NEB 5-alpha F' Iq Competent E. coli suitable for toxic genes (NEB Ipswich, MA) according to the manufacturer's protocol.

pCDH-EF1a-MCS-T2A-copGFP vector was purchased from SBI system biosciences (Mountain View, CA) to allow for efficient bi-cistronic expression[51]. *SCD1* previously cloned from cDNA was amplified with primers carrying restriction enzymes sequences as following: NheI for 5' amplification (5'-GCTAGCGCCACCATGCCGGCCCACTTGCTG-3') and Bam HI for 3' amplification (5'-GGATCCGCCACTCTTGTAGTTTCCATC-3'). Purified inserts and the pCDH-EF1a-MCS-T2A-copGFP vector were digested and with NheI and BamHI restriction enzymes and ligated to form pCDH-EF1a-SCD1-T2A-copGFP**.** The backbone of the vector (pCDH-EF1a-MCS-T2A-copGFP) was used as the control vector.

Patient samples

Primary patient material was obtained from approved biobanks. ALL live cells from diagnosis – Bloodwise Childhood Leukaemia Cell Bank, normal control CSF – Glasgow Neuroimmunology Biobank, ALL patient CSF – West of Scotland CSF Biobank, plasma – NHS Greater Glasgow & Clyde Bio-repository. Use of biobanked human samples for this specific project was approved by the West of Scotland Research Ethics Service (ref 09/S0703/77). All research was conducted in accordance with the Declaration of Helsinki.

Xenotransplants

JAX NOD.Cg-Prkdcscidll2rgtm1Wjl/SzJ (NSG; Charles River Laboratories, Harlow, United Kingdom) mice were kept in sterile isolators with autoclaved food, bedding, and water. Xenotransplants were performed in 6-10 weeks old mice, the experimental protocol varied according to the model, with details given in **Supplementary Table 3**. At the end of experiment, mice were sacrificed by overdose of pentobarbital (IP) and cells were collected from bone marrow, spleen and leptomeninges as previously described[17]. For RNA sequencing leukemic cells were purified using a Ficoll gradient (Lymphoprep, Stemcell) following the supplier instructions. Purity was determined using flow cytometry. Cells were dry pelleted and snap frozen for further use (see below). For *SCD1* overexpression and inhibition experiments bone marrow, spleen and leptomeningeal cells were analyzed to check human engraftment by FACS using Absolute counting beads (Beckman Coulter). GFP was used to identify human cells. The tumor load was expressed as total amount of leukemic cells in each organ. Competition assays were performed by transplanting SCD1 overexpressing and control

cells in the same mouse in a 1:1 ratio ($1.25x10^6$ cells/type, total $2.5x10^6$ cells/mouse). Patient's samples (PDXs) were expanded in NSG mice and experiments were performed upon secondary-tertiary passage in the mice. $1x10^6$ cells from donor mice (90% human engraftment) were transplanted in recipients to perform the experiments.

All animal experiments were approved by Institutional Ethical Review Process Committees and were performed under UK Home Office license (PPL 60-4512), Israel Institutional Animal care and use committee approval (1074/16/ANIM) and Institutional Animal Care and use Committee at Memorial Sloan Kettering Cancer Center (protocol 11-10-025).

FBS delipidation using fumed silica

The protocol for delipidation of FBS was adapted from Agnese et al. (1983)[52]. Lipid depletion was achieved by adding two grams of fumed silica (Sigma Aldrich) to 100 mL of FBS, and the suspension was stirred for 2h30. Centrifugation at 5000 rpm for 35 minutes, at room temperature. The supernatant was filtered through a 0.45 µm filter at first, and then through a 0.22 µm filter.

***In vitro* treatment with the SCD1 inhibitor SW203668**

At day 0, $0.5x10^6$ cells were seeded in RPMI supplemented with lipidated or delipidated FBS. A concentration of 1 µM of the SCD1 inhibitor SW203668 or of the vehicle (DMSO) was added daily, over 96h.

In vivo treatment with the SCD1 inhibitor SW203668

Ten 6-week old NSG females were transplanted with $1.5x10^6$ $GFP^+mCherry^+FFLuc^+$ 018z cells. Treatment started 24 hours after transplantation with five mice receiving vehicle (10% DMSO+ 10% Kolliphor (Sigma Aldrich) + 80% lactic acid pH 5.5) and 5 other mice receiving the small molecule SCD1 inhibitor SW203668 (Cayman Chemical) at 20 mg/kg twice a day I.P. for 10 days. *In vivo* bioluminescence assay (IVIS Lumina LT, Series III, Caliper Life Sciences) was performed at day 10, immediately before sacrifice. Secondary and tertiary PDXs were transplanted into 6 weeks old NSG female mice at a dose of $1x10^6$ cells. The treatment with 20 mg/kg SW203668 started 1 week after the transplant. Mice were sacrificed when they showed the first signs of sickness. Details on time of treatment for each PDX are displayed in **Supplementary Table 3**. Bone marrow, spleen and meninges were collected post-mortem and analysed to check human engraftment by FACS using absolute counting beads (Beckman Coulter). GFP expression was used to identify human cells. The tumor load was expressed as total amount of leukemic cells in each organ.

SCD1 intracellular staining

Cells isolated from bone marrow and CNS of mice transplanted with human leukemic cells were fixed with PFA 1.6% and permeabilized with ice-cold 90% methanol. GFP was used to gate on human cells. Rabbit anti human monoclonal SCD1 antibody (SCD1

515 ($C_{12}H_5$) Rabbit mAb #2794, Cell Signaling) was used at a dilution of 1:50 in PBS for 20
516 minutes at 4°C.

517

518 **Western blot**

519 SCD1-high and low cells were cultured in RPMI supplemented with 20% FBS and
520 harvested in PBS, then pelleted and lysed in CelLytic™ MT Cell Lysis Reagent (Sigma
521 Aldrich) supplemented with complete mini protease cocktail (11836153001 Roche) and
522 phosphatase inhibitor cocktail (200-664-3 Sigma Aldrich). Cells were incubated on ice
523 for 30 minutes before clarification. Standard procedures were used for western blotting.
524 Fifty µg of total protein lysate were loaded on a 12% Polyacrylamide gel and incubated
525 overnight with rabbit anti-human monoclonal SCD1 antibody 1:2000 (SCD1 ($C_{12}H_5$)
526 Rabbit mAb #2794, Cell Signaling) and vinculin (Vinculin Antibody #4650, Cell
527 Signaling) at 4°C. Proteins were detected using ECL Western Blotting Substrate
528 (Promega).

529

530 **CSF and plasma sampling from mice**

531 CSF was collected from mice under terminal anesthesia with pentobarbital. A 25-gauge
532 needle was percutaneously inserted into the cisterna magna and CSF collected by
533 gravity. Blood was collected immediately post-mortem. Both CSF and blood were
534 centrifuged at 2,000g for 15 min at 4°C. CSF supernatant and plasma were snap-frozen
535 and stored at −80°C until analysis.

Gas Chromatography/Mass Spectrometry analyses

CSF or plasma samples were precipitated vol/vol with ice-cold glacial MetOH (15min, -20°C), followed by ice-cold glacial chloroform extraction (ratio 1:3). After centrifugation (13,000rpm, 5min), the chloroform fraction was extracted into GC-MS glass vials (Agilent). Samples were dried under nitrogen and stored at -20°C for subsequent use. On the day of analysis, samples were re-suspended in chloroform/MetPrepII solution to generate fatty acid methyl esters (FAMEs). Samples were analyzed using an Agilent 7890B GC system coupled with an Agilent 7000 Triple Quadrupole mass spectrometer. Phenomenex ZB-1701P columns (30 m × 0.25 mm × 0.25 µm) were used for FAME separation. Further details are given in **Supplementary Table 4**. Generated data files were pre-processed with Agilent Mass Hunter B.06.00 software and relative intensities of FAMEs were extracted using R-based script MetabQ[53]. Absolute quantities of fatty acids were calculated using the calibration curves.

Liquid Chromatography/Mass Spectrometry analyses

Plasma and CSF samples were diluted 50-fold with cold solvent, comprising 50% methanol, 30% acetonitrile, 20% water. Free fatty acids and fatty acid precursors were extracted from CNS and bone marrow cells, and from $1x10^6$ cells from *in vitro* culture, by resuspending cells in 1mL of the same solvent. Samples were vortexed for 15min and then centrifuged at 16,100 x g for 10 minutes at 0-4°C. Supernatants were transferred to glass HPLC vials and kept at -80°C prior to LC-MS analysis.

Total fatty acids were extracted from $1x10^6$ *in vitro* cultured cells. For lipid saponification, cells were resuspended in 1 mL of 90% methanol in water containing 0.3M of potassium hydroxide, followed by vortexing and incubation at 80ºC for 60 minutes. Samples were then brought to room temperature and 100 µL of formic acid and 800 µL of hexane were added to each sample. After vortexing, the upper phase was transferred into a glass HPLC vial, and samples were re-extracted with 700 µL of hexane. The upper phase was again collected and pooled with previously collected volume. Samples were dried under nitrogen, reconstituted in 200 µL of methanol, and stored at -80°C until LC-MS analysis. Fatty acids were analyzed by a QExactive Orbitrap mass spectrometer (Thermo Scientific, Waltham, MA, USA) together with a Thermo Ultimate 3000 HPLC system. The HPLC setup consisted of a HSS T3 column (150 x 2.1 mm, 1.8 µm, Waters Corporation, Milford, MA, USA), with a HSS T3 guard column (Waters, 1.8 µm) and an initial mobile phase of 80% 0.1% formic acid in water/ 20% 0.1% formic acid in acetonitrile. Samples (5 µl) were injected and metabolites were separated over a 7 minutes mobile phase gradient, increasing the organic mobile phase (0.1% formic acid in acetonitrile) to 95%, using a flow rate of 400 µL/min and a column temperature of 45°C. The total analysis time was 12 minutes.

For fatty acyl-CoAs extraction, $8x10^6$ cells cultured *in vitro* were resuspended in 700 µL of cold methanol (-20ºC). The samples were vigorously vortexed for 60 seconds and put at -20ºC for 10 minutes. 500 µL of cold (-20ºC) chloroform were added to the tube and the mixture was vigorously vortexed for 60 seconds. Then, 270 µL of water were added

to the mixture, the samples were vortexed again and placed on ice for 10 min. Tubes were centrifuged at 4ºC, 16,100 x *g* for 15 minutes. 500 µL of the upper layer were transferred into 1 mL glass vial and gently dried under nitrogen. The dried extracts were reconstituted in 50 µL of methanol:water (in a proportion of 1:1) and transferred to HPLC glass vials equipped with 50 µL inserts. Thermo Ultimate 3000 high-performance liquid chromatography (HPLC) system coupled to Q- Exactive Orbitrap Mass Spectrometer (Thermo Fisher Scientific) was used with a resolution of 70,000 at 200 mass/charge ratio (m/z), with electrospray ionization. Detection was at positive mode across a mass range of 600 to 1500 m/z. HPLC setup consisted HSS T3 column (150 x 2.1 mm, 1.8 µm, Waters). 5 µL of biological extracts were injected and the compounds were separated with mobile phase gradient of 12 min, starting at 90% aqueous (0.5% Ammonium hydroxide) and 10% organic (Acetonitrile with 0.5% Ammonium hydroxide) and terminated with 40% organic. Flow rate and column temperature were maintained at 0.3 mL/min and 30°C, respectively, for a total run time of 18 min. HESI source parameters: the sheath gas flow rate and the aux gas flow rate were set to 45 and 10 arbitrary units; the spray voltage was 4.5 Kv; The capillary temperature and the aux gas heater temperature were 300c and 350c respectively; the S-lens RF level was set at 50. All metabolites were detected using mass accuracy below 5 ppm. Thermo Xcalibur was used for data acquisition. TraceFinder 4.1 was used for analysis. Peak areas of metabolites were determined by using the exact mass of the singly charged ions.

Reverse transcription and quantitative Real Time Polymerase Chain Reaction (qPCR)

RNA was extracted from cells resuspended and lysed in TRIzol according to manufacturer's instructions, and underwent DNase treatment using an RNase-free DNase kit (Qiagen). RNA quality was assessed with the RNA Nano Chip kit (Agilent) on an Agilent Bioanalyser 2100. 5 µg of total RNA from each sample was used to synthesize cDNA using the PrimeScript RT reagent kit (Promega) with oligo-dT primers, according to the manufacturer's instructions. Quantitative PCR reactions were performed with specific primers listed in **Supplementary Table 5** and the GoTaq qPCR master mix kit (Promega) using the Biorad system. Differential expressions of transcripts of interest were calculated in relation to the human 36B4 housekeeping transcript for SEM and REH cell line. For 018z cell line, quantitative PCR reactions were performed with the SYBR™ Green PCR Master Mix (Thermo Fisher) using the StepOnePlus™ Real-Time PCR System (Applied Biosystems). Human HPRT was used as a housekeeping gene.

For patient-derived xenograft samples cDNA was generated using Applied Biosystems High-Capacity RNA-to-cDNA™ Kit (Thermo Fisher, MA, #4387406). cDNA was amplified in a sequence-specific manner using a Multiplex PCR kit (Qiagen # 206143), then treated with Exonuclease I (4U/µL New England Biolabs, MA, #M0293L) to remove unincorporated primers. Samples and primers were loaded onto a 48.48 Dynamic Array™ chip. The chip was primed on a Biomark™ IFC controller MX then multiplex PCR performed using a Biomark™ system for Genetic Analysis (all Fluidigm Corporation, CA). All steps were performed as per manufacturer's instructions. Data were analysed using the comparative CT method[54].

627

628 **RNA sequencing analyses**

629 RNA samples were run on a Next Seq500 Sequencing system (Illumina). The raw fastq
630 files containing paired-end 2 x 75bp reads were pre-processed to trim the 3' end
631 adapter with Cutadapt[55] (version 1.5) and to trim the very low quality reads using Sickle
632 (version 0.940) software (https://github.com/najoshi/sickle) with generous quality
633 threshold -q 10. Only read pairs containing ≥54 bases were kept. Transcript expression
634 quantification was performed using Kallisto (version 0.42.4) software[56] against
635 combined human and mouse transcriptomes, Ensembl GRCh38 and GRCm38,
636 respectively, in order to remove the possible mouse RNA contamination. Read counts
637 related to human transcripts were collected, rounded, and summarized into gene
638 specific read counts. These were then processed with DESeq2 software[57] to generate
639 gene expression estimates after regularized log transformation which stabilized
640 variance as a function of mean.

641

642 **Metabolic enrichment**

643 Preprocessed RNA expression data from RNA sequencing was analyzed using single
644 sample gene set enrichment analysis (ssGSEA). Gene expression signatures for
645 metabolic pathways were downloaded from the MSIGDB database
646 (software.broadinstitute.org/gsea/msigdb) and included signatures from the KEGG and
647 REACTOME pathway databases. For each signature *S* and each sample, a positive
648 signature score was calculated together with a *p*-value p_S indicating the significance of

649 the score (permutation test, n=10,000). For a given signature *S*, we calculated the fold
650 change in the expression of the signature between the two sample groups (CNS,
651 Spleen) as the difference of the log-transformed p-values E_S(sample)=-$\log_2$(p_S(sample)),
652 i.e. *FC(S)*=mean(E_S(*CNSsamples*))-mean(E_S(*SPLEENsamples*)). The fold changes
653 were plotted in a bar plot. *Student's T-test* was used to calculate significance of
654 differential expression between the groups. Furthermore, a Pre-Ranked GSEA using
655 fold change values was performed to display the enrichment profiles for several gene-
656 sets (permutation test, n=1,000, classic enrichment statistic). All the regular log-
657 transformed counts of selected genes were double-scaled. The biclustering was
658 performed using Euclidean distance and complete linkage and the heatmap was made
659 using the gplots package for R (v. 3.0.1)[58].

660

661 For comparison, available human and primograft data was downloaded from the GEO
662 database (https://www.ncbi.nlm.nih.gov/geo/), Refs. GSE60926 and GSE89710
663 respectively. Those datasets were analysed using the Affymetrix Transcriptome
664 Analysis Console v4.0, employing Robust Multiarray Average summarization and the
665 moderated differential expression analysis was carried out using the empirical Bayes
666 method with FDR correction.

667

668 **Histology**

669 Murine heads and femurs were stripped of soft tissues, fixed in 10% neutral buffered
670 formalin (CellPath, Powys, United Kingdom), and decalcified in Hilleman and Lee EDTA

671 solution (5.5% EDTA in 10% formalin) for 2 to 3 weeks. Following paraffin embedding,
672 hematoxylin and eosin staining (Sigma-Aldrich) was performed on 5-mm brain/femur
673 sections. Photographs were taken using an Axio Observer Light microscope (Zeiss).

674

675 **Statistical analysis**

676 Parametric data were analyzed using two-sided Student unpaired or paired t-tests.
677 Nonparametric data were analyzed using two-sided Mann-Whitney U tests. For wet lab
678 experiments a p value of <0.05 was considered significant. In all figures, data are
679 presented as Mean ± Standard Deviation (SD). Analysis was carried out using
680 GraphPad Prism software (La Jolla, CA).

681

682 **Data availability**

683 RNA-seq data supporting the findings of this study have been deposited in Gene Bank
684 (accession numbers: GSE135115; GSE135113; GSE135114). The GSE135115
685 SuperSeries is entitled "Gene expression profiles of MLL-AF4 and TEL-AML1 acute
686 lymphoblastic leukaemia blasts retrieved from central nervous system and spleen". This
687 SuperSeries contains two series related to SEM and REH experiments as follows:
688 GSE135113 "Gene expression profiles of MLL-AF4 acute lymphoblastic leukaemia
689 blasts retrieved from central nervous system and spleen", GSE135114 "Gene
690 expression profiles of TEL-AML1 acute lymphoblastic leukaemia blasts retrieved from
691 central nervous system and spleen". The source data associated with each figure is

provided with the manuscript. All other data supporting the findings of this study is available from the corresponding author on reasonable request.

ACKNOWLEGMENTS

We thank the patients and their families who generously donated the samples used in this study to the NHS Greater Glasgow and Clyde Biorepository, Laboratory Medicine Building, Queen Elizabeth University Hospital (QEUH), the Bloodwise Childhood Leukaemia Cellbank, the Glasgow Neuroimmunology Biobank and the West of Scotland CSF biobank. In addition, we thank John Goodfellow, Hugh Willison, Saeeda Bhatti and Yasar Yousafzai for assistance with obtaining primary samples, Clare Orange and Lynn Stevenson for help with histology. Histology slides were scanned by University of Glasgow slide scanning and image analysis service at the QEUH. RNA sequencing was performed by the Glasgow Polyomics research facility at the University of Glasgow. We also thank Karen Keeshan and the Biological Services Unit, Cancer Research UK Beatson Institute of Cancer Research for animal assistance.

This work was supported by the Chief Scientist Office (O.O. and C.H. Grant ETM/374), Fondazione Italiana per la Ricerca sul Cancro *FIRC (A.M.S.), the William and Elizabeth Davies Foundation (A.C. – Clinical research fellowship), the Laura and Ike Perlmutter Fund (E.G. and I.A.), the German Israel Foundation (A.Z.) and the Israel Science Foundation 1775/12 (E.G., I.M.). This project has received funding from the European Union's Horizon 2020 research and innovation programme under the Marie

Skłodowska-Curie grant agreement META-CAN No 766214 (S.I.F., J.F-G., I.M. and E.G.).

AUTHORS CONTRIBUTION

A.M.S., S.I.F., O.O., E.G., C.H., P.H., S.I. designed the study. A.M.S., S.I.F., O.O., A.C., A.Z., S.B., I.G., L.F., Y.B., C.E., performed most of the experiments. A.M.S., S.I.F., O.O., A.C., P.H., E.K.M., J.G-F., C.H., I.M., E.G. analyzed and interpreted the data. S.T., I.A., J.J.K. and G.M. performed and analyzed the mass spectrometry experiments. A.M.S., S.I.F., O.O., C.H., E.G., I.M. and S.I. wrote the manuscript.

REFERENCES

1. Cairns, R. A., Harris, I. S. & Mak, T. W. Regulation of cancer cell metabolism. *Nat. Rev. Cancer* **11**, 85–95 (2011).
2. DeBerardinis, R. J. & Chandel, N. S. Fundamentals of cancer metabolism. *Sci. Adv.* **2**, 1–18 (2016).
3. Cha, J.-Y. & Lee, H.-J. Targeting Lipid Metabolic Reprogramming as Anticancer Therapeutics. *J. Cancer Prev.* **21**, 209–215 (2017).
4. Gisselbrecht, C. Positron emission tomography – Guided therapy of aggressive non-hodgkin lymphoma: Standard of care after the PETAL study? *J. Clin. Oncol.* **36**, 3272–3273 (2018).
5. Caro, P. *et al.* Metabolic Signatures Uncover Distinct Targets in Molecular Subsets of Diffuse Large B Cell Lymphoma. *Cancer Cell* **22**, 547–560 (2012).
6. Kuntz, E. M. *et al.* Targeting mitochondrial oxidative phosphorylation eradicates therapy-resistant chronic myeloid leukemia stem cells. *Nat. Med.* **23**, 1234–1240 (2017).
7. Nachmias, B. & Schimmer, A. D. Metabolic Flexibility in Leukemia—Adapt or Die. *Cancer Cell* **34**, 695–696 (2018).
8. Olivares, O., Däbritz, J. H. M., King, A., Gottlieb, E. & Halsey, C. Research into cancer metabolomics: Towards a clinical metamorphosis. *Semin. Cell Dev. Biol.* **43**, 52–64 (2015).

9. Frishman-Levy, L. & Izraeli, S. Advances in understanding the pathogenesis of CNS acute lymphoblastic leukaemia and potential for therapy. *Br. J. Haematol.* **176**, 157–167 (2017).

10. Pui, C. H. & Howard, S. C. Current management and challenges of malignant disease in the CNS in paediatric leukaemia. *Lancet Oncol.* **9**, 257–268 (2008).

11. Halsey, C. *et al.* The impact of therapy for childhood acute lymphoblastic leukaemia on intelligence quotients; Results of the risk-stratified randomized central nervous system treatment trial MRC UKALL XI. *J. Hematol. Oncol.* **4**, 1–12 (2011).

12. Iyer, N. S., Balsamo, L. M., Bracken, M. B. & Kadan-Lottick, N. S. Chemotherapy-only treatment effects on long-term neurocognitive functioning in childhood ALL survivors: A review and meta-analysis. *Blood* **126**, 346–353 (2015).

13. Price, R. A. & Johnson, W. W. The central nervous system in childhood leukemia: I. The arachnoid. *Cancer* **31**, 520–533 (1973).

14. Münch, V. *et al.* Central nervous system involvement in acute lymphoblastic leukemia is mediated by vascular endothelial growth factor. *Blood* **130**, 643–654 (2017).

15. van der Velden, V. H. J. *et al.* New cellular markers at diagnosis are associated with isolated central nervous system relapse in paediatric B-cell precursor acute lymphoblastic leukaemia. *Br. J. Haematol.* **172**, 769–781 (2016).

16. Krause, S. *et al.* Mer tyrosine kinase promotes the survival of t(1;19)-positive acute lymphoblastic leukemia (ALL) in the central nervous system (CNS). *Blood* **125**, 820–830 (2015).

17. Williams, M. T. S. *et al.* The ability to cross the blood-cerebrospinal fluid barrier is a generic property of acute lymphoblastic leukemia blasts. *Blood* **127**, 1998–2006 (2016).

18. Williams, M. T. S. *et al.* Interleukin-15 enhances cellular proliferation and upregulates CNS homing molecules in pre-B acute lymphoblastic leukemia. *Blood* **123**, 3116–3127 (2014).

19. Buonamici, S. *et al.* CCR7 signalling as an essential regulator of CNS infiltration in T-cell leukaemia. *Nature* **459**, 1000–1004 (2009).

20. Frishman-Levy, L. *et al.* Central nervous system acute lymphoblastic leukemia: Role of natural killer cells. *Blood* **125**, 3420–3431 (2015).

21. Spector, R., Robert Snodgrass, S. & Johanson, C. E. A balanced view of the cerebrospinal fluid composition and functions: Focus on adult humans. *Exp. Neurol.* **273**, 57–68 (2015).

22. Hühmer, A. F., Biringer, R. G., Amato, H., Fonteh, A. N. & Harrington, M. G. Protein Analysis in Human Cerebrospinal Fluid: Physiological Aspects, Current Progress and Future Challenges. *Dis. Markers* **22**, 3–26 (2006).

23. Damkier, H. H., Brown, P. D. & Praetorius, J. Cerebrospinal Fluid Secretion by the

Choroid Plexus. *Physiol. Rev.* **93**, 1847–1892 (2013).

24. Méndez-Ferrer, S. *et al.* Mesenchymal and haematopoietic stem cells form a unique bone marrow niche. *Nature* **466**, 829–834 (2010).

25. Morrison, S. J. & Scadden, D. T. The bone marrow niche for haematopoietic stem cells. *Nature* **505**, 327–334 (2014).

26. Olechnowicz, S. W. Z. & Edwards, C. M. Contributions of the host microenvironment to cancer-induced bone disease. *Cancer Res.* **74**, 1625–31 (2014).

27. Eckhoff, E. M., Queudeville, M., Debatin, K.-M. & Meyer, L. H. A novel B cell precursor ALL cell line (018Z) with prominent neurotropism and isolated CNS leukemia in a NOD/SCID/huALL xenotransplantation model. *Blood* **114**, 1630–1630 (2009).

28. Theodoropoulos, P. C. *et al.* Discovery of Tumor-Specific Irreversible Inhibitors of Stearoyl CoA Desaturase. *Nat Chem Biol* **12**, 218–225 (2016).

29. Bartram, J. *et al.* High throughput sequencing in acute lymphoblastic leukemia reveals clonal architecture of central nervous system and bone marrow compartments. *Haematologica* **103**, e110–e114 (2018).

30. Metallo, C. M. *et al.* Reductive glutamine metabolism by IDH1 mediates lipogenesis under hypoxia. *Nature* **481**, 380–384 (2012).

31. Angelucci, C. *et al.* Pivotal role of human stearoyl-CoA desaturases (SCD1 and 5) in breast cancer progression: oleic acid-based effect of SCD1 on cell migration and a novel pro-cell survival role for SCD5. *Oncotarget* **9**, 24364–24380 (2018).

32. Hess, D., Chisholm, J. W. & Igal, R. A. Inhibition of stearoylCoA desaturase activity blocks cell cycle progression and induces programmed cell death in lung cancer cells. *PLoS One* **5**, e11394 (2010).

33. Wang, J. *et al.* High expression of Stearoyl-CoA desaturase 1 Predicts Poor Prognosis in Patients with Clear-Cell Renal Cell Carcinoma. *PLoS One* **11**, e0166231 (2016).

34. Chen, L. *et al.* Stearoyl-CoA desaturase-1 mediated cell apoptosis in colorectal cancer by promoting ceramide synthesis. *Sci. Rep.* **6**, 1–11 (2016).

35. Kim, S. J., Choi, H., Park, S. S., Chang, C. & Kim, E. Stearoyl CoA desaturase (SCD) facilitates proliferation of prostate cancer cells through enhancement of androgen receptor transactivation. *Mol. Cells* **31**, 371–377 (2011).

36. Zhang, H., Li, H., Ho, N., Li, D. & Li, S. Scd1 Plays a Tumor-Suppressive Role in Survival of Leukemia Stem Cells and the Development of Chronic Myeloid Leukemia. *Mol. Cell. Biol.* **32**, 1776–1787 (2012).

37. Southam, A. D. *et al.* Drug redeployment to kill leukemia and lymphoma cells by disrupting SCD1-mediated synthesis of monounsaturated fatty acids. *Cancer Res.* **75**, 2530–2540 (2015).

38. Imamura, K. *et al.* Discovery of Novel and Potent Stearoyl Coenzyme A

Desaturase 1 (SCD1) Inhibitors as Anticancer Agents. *Bioorganic Med. Chem.* **25**, 3768–3779 (2017).

39. Folger, O. *et al.* Predicting selective drug targets in cancer through metabolic networks. *Mol. Syst. Biol.* **7**, 1–10 (2011).

40. Miyazaki, M., Man, W. C. & Ntambi, J. M. Targeted Disruption of Stearoyl-CoA Desaturase1 Gene in Mice Causes Atrophy of Sebaceous and Meibomian Glands and Depletion of Wax Esters in the Eyelid. *J. Nutr.* **131**, 2260–2268 (2001).

41. Brown, J. M. & Rudel, L. L. Stearoyl-coenzyme A desaturase 1 inhibition and the metabolic syndrome: considerations for future drug discovery. *Curr Opin Lipidol* **21**, 192–197 (2010).

42. Vriens, K. *et al.* Evidence for an alternative fatty acid desaturation pathway increasing cancer plasticity. *Nature* **566**, 403–406 (2019).

43. Ono, A. *et al.* Feedback activation of AMPK-mediated autophagy acceleration is a key resistance mechanism against SCD1 inhibitor-induced cell growth inhibition. *PLoS One* **12**, e0181243 (2017).

44. Hagedorn, N. *et al.* Submicroscopic bone marrow involvement in isolated extramedullary relapses in childhood acute lymphoblastic leukemia: a more precise definition of “isolated” and its possible clinical implications, a collaborative study of the Resistant Disease Committee . *Blood* **110**, 4022–4029 (2007).

45. Yuneva, M. O. *et al.* The metabolic profile of tumors depends on both the responsible genetic lesion and tissue type. *Cell Metab.* **15**, 157–170 (2012).

46. Hensley, C. T. *et al.* Metabolic Heterogeneity in Human Lung Tumors. *Cell* **164**, 681–694 (2016).

47. Kerr, E. M., Gaude, E., Turrell, F. K., Frezza, C. & Martins, C. P. Mutant Kras copy number defines metabolic reprogramming and therapeutic susceptibilities. *Nature* **531**, 110–113 (2016).

48. Sciacovelli, M. & Frezza, C. Metabolic reprogramming and epithelial-to-mesenchymal transition in cancer. *FEBS J.* **284**, 3132–3144 (2017).

49. Burrell, R. A., McGranahan, N., Bartek, J. & Swanton, C. The causes and consequences of genetic heterogeneity in cancer evolution. *Nature* **501**, 338–345 (2013).

50. Sanjana, N. E., Shalem, O. & Zhang, F. Improved vectors and genome-wide libraries for CRISPR screening. *Nat. Methods* **11**, 783–784 (2014).

51. Ibrahimi, A. *et al.* Highly efficient multicistronic lentiviral vectors with peptide 2A sequences. *Hum. Gene Ther.* **20**, 845–860 (2009).

52. Agnese, S. T., Spierto, F. W. & Hannon, W. H. Evaluation of four reagents for delipidation of serum. *Clin. Biochem.* **16**, 98–100 (1983).

53. Tumanov, S. *et al.* Calibration curve-free GC–MS method for quantitation of amino and non-amino organic acids in biological samples. *Metabolomics* **12**, 1–13 (2016).

54. Schmittgen, T. D. & Livak, K. J. Analyzing real-time PCR data by the comparative CT method. *Nat. Protoc.* **3**, 1101–8 (2008).

55. Martin, M. & N, T. Cutadapt removes adapter sequences from high-throughput sequencing reads. *EMBnet.journal* (2011).

56. Bray, N. L., Pimentel, H., Melsted, P. & Pachter, L. Near-optimal probabilistic RNA-seq quantification. *Nat. Biotechnol.* **34**, 525–527 (2016).

57. Love, M. I., Huber, W. & Anders, S. Moderated estimation of fold change and dispersion for RNA-seq data with DESeq2. *Genome Biol.* **15**, 1–21 (2014).

58. Warnes, G. R. *et al.* gplots: Various R Programming Tools for Plotting Data. R package version 3.0-1. *http://CRAN.R-project.org/package=gplots.* (2015).

874

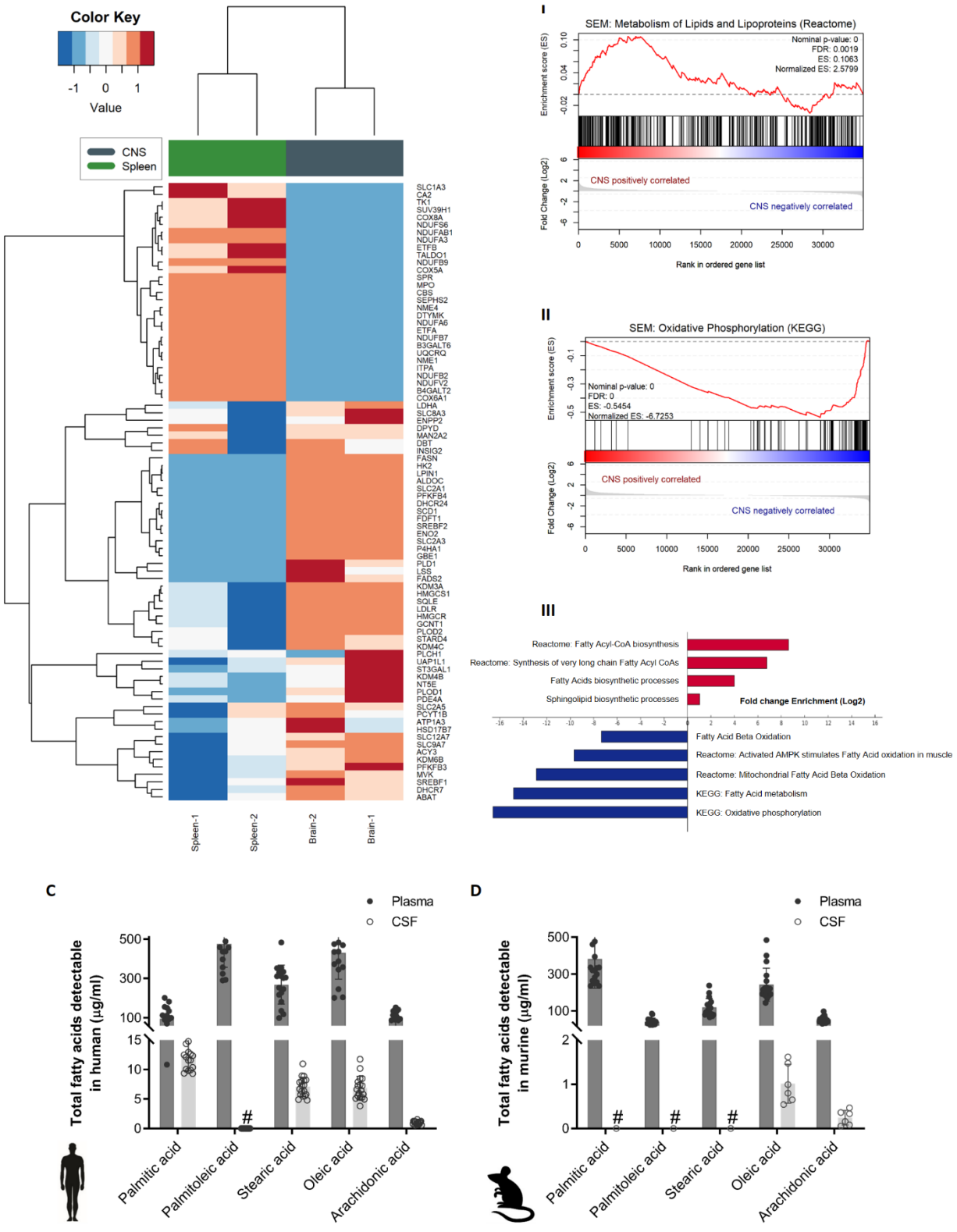
Color Key
-1 0 1
Value
CNS
Spleen
Spleen-1
Spleen-2
Brain-2
Brain-1
I
SEM: Metabolism of Lipids and Lipoproteins (Reactome)
Nominal p-value: 0
FDR: 0.0019
ES: 0.1063
Normalized ES: 2.5799
Enrichment score (ES)
CNS positively correlated
CNS negatively correlated
Fold Change (Log2)
Rank in ordered gene list
II
SEM: Oxidative Phosphorylation (KEGG)
Nominal p-value: 0
FDR: 0
ES: -0.5454
Normalized ES: -6.7253
III
Reactome: Fatty Acyl-CoA biosynthesis
Reactome: Synthesis of very long chain Fatty Acyl CoAs
Fatty Acids biosynthetic processes
Sphingolipid biosynthetic processes
Fold change Enrichment (Log2)
Fatty Acid Beta Oxidation
Reactome: Activated AMPK stimulates Fatty Acid oxidation in muscle
Reactome: Mitochondrial Fatty Acid Beta Oxidation
KEGG: Fatty Acid metabolism
KEGG: Oxidative phosphorylation
C
Plasma
CSF
Total fatty acids detectable in human (µg/ml)
Palmitic acid
Palmitoleic acid
Stearic acid
Oleic acid
Arachidonic acid
D
Total fatty acids detectable in murine (µg/ml)

875

876 **FIGURE 1**

Figure 1. Fatty acid synthesis-related genes are upregulated in CNS-derived ALL cells in xenograft models. (A) Heatmap representation of hierarchical clustering of genes differentially expressed between human SEM cells isolated from CNS and spleen of xenografted mice (n=2 independent groups of 5 mice). **(B)I-II** Enrichment plots of metabolism of lipids and lipoproteins (REACTOME) and oxidative phosphorylation (KEGG) for SEM cell line extracted from the CNS and spleen of xenografted mice. Profile of the running ES score & Positions of the GeneSet Members on the Rank Ordered List. **III** Statistically significant biological functions in SEM cells isolated from CNS and spleen of xenografted mice. Single sample GSEA scores were calculated for an array of metabolic gene signatures from MSIGDB, including KEGG, Reactome and GO term signatures. p-values for positive association with a signature (enrichment) were calculated by permutation test. Plotted are signatures with significant fold-changes in enrichment between the CNS versus spleen groups (log_2 scale). Red bars indicate signatures with positive log fold-change (gain) in CNS versus spleen, blue bars indicate negative log fold-change (loss) in CNS versus spleen samples. **(C)** Total fatty acid levels measured by GC-MS in non-leukemic human plasma and CSF samples. n=18. Bars represent mean +/- SD. #: below detection levels. **(D)** Total fatty acid levels measured by GC-MS in non-leukemic murine plasma and paired CSF samples. n=9. Bars represent mean +/- SD. #: below detection levels.

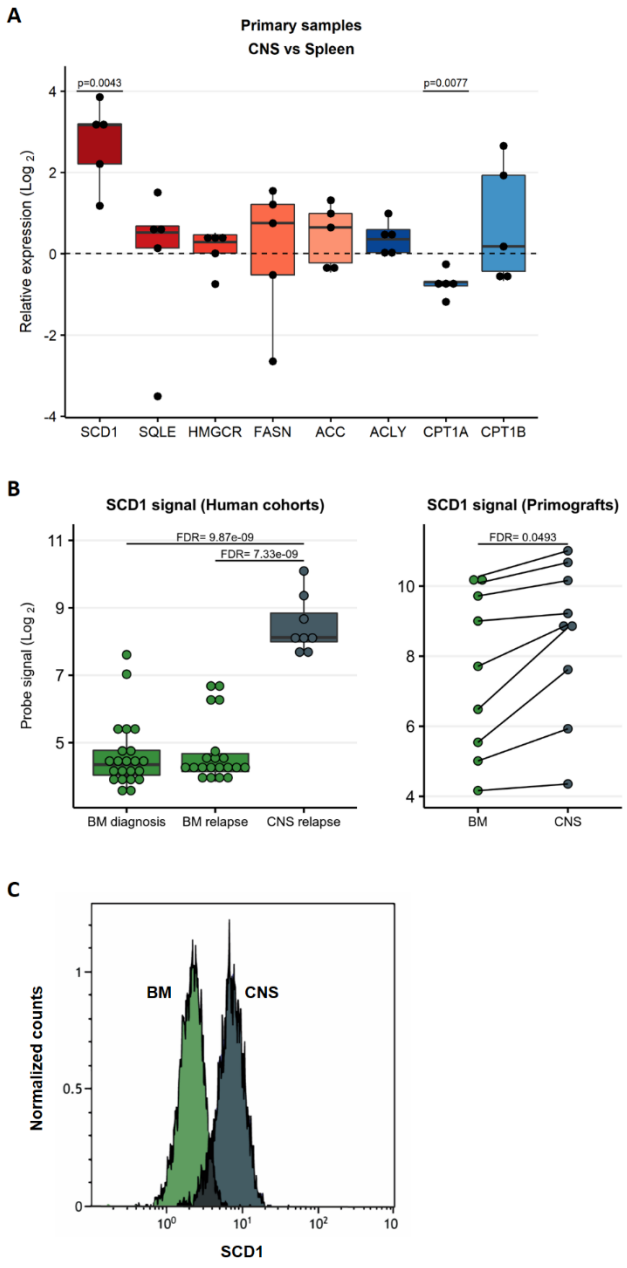
A
Primary samples
CNS vs Spleen
p=0.0043
p=0.0077
Relative expression (Log 2)
SCD1
SQLE
HMGCR
FASN
ACC
ACLY
CPT1A
CPT1B
B
SCD1 signal (Human cohorts)
FDR= 9.87e-09
FDR= 7.33e-09
Probe signal (Log 2)
BM diagnosis
BM relapse
CNS relapse
SCD1 signal (Primografts)
FDR= 0.0493
BM
CNS
C
Normalized counts
BM
CNS
SCD1

FIGURE 2

Figure 2. SCD1 is upregulated in primary patient samples in the central nervous system. (A) Quantitative PCR validation of top ranked genes from RNA-Seq in n=5 patient derived xenografts with t(12;21) ETV6-RUNX1 (TEL-AML1) translocation or t(4;11) MLL-AFF1 (MLL-AF4)] translocation. Results are normalized to 36B4 human housekeeping gene and presented as Log_2 fold change enrichment comparing CNS to spleen. p (two tailed) = One sample T and Wilcoxon test. **(B)** Gene expression of *SCD1* from RNAseq data deposited in public databases. Left: Samples of BM of patients at diagnosis and relapse and CNS at relapse, unpaired analysis. Right: Patient-derived xenograft samples established by transplantation of patients' ALL cells onto NSG mice. *SCD1* expression in cells isolated from paired CNS and spleen is shown in the graph. FDR – False discovery rate**. (C)** Intracellular staining of *SCD1* in cells from the BM (green) and CNS (grey) of a mouse transplanted with 018z cells. The peaks are relative to the percentage of human $CD19^+$ cells normalized to mode.

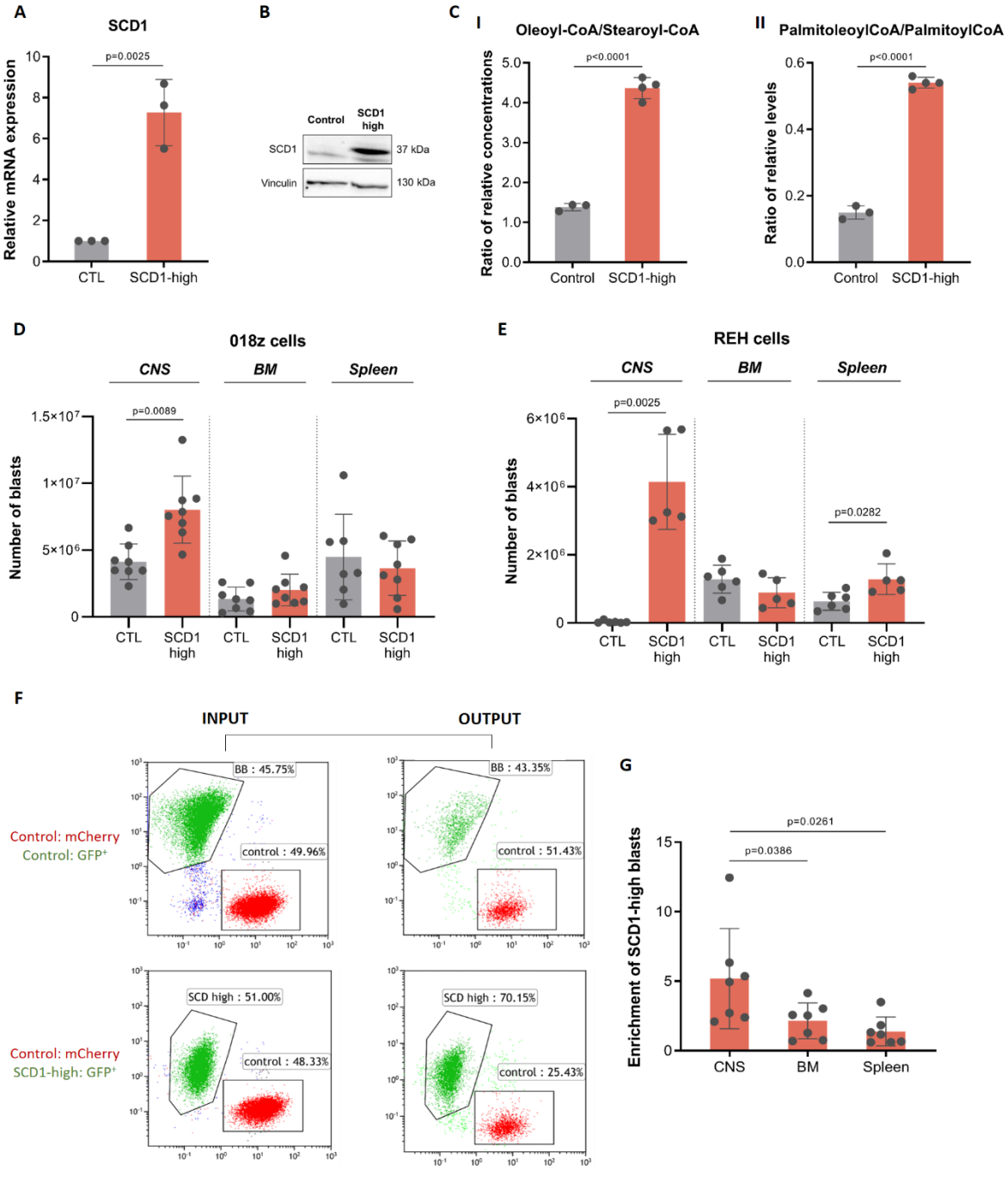
A
SCD1
p=0.0025
Relative mRNA expression
CTL
SCD1-high
B
Control
SCD1 high
SCD1
37 kDa
Vinculin
130 kDa
C
I
Oleoyl-CoA/Stearoyl-CoA
p<0.0001
Ratio of relative concentrations
Control
SCD1-high
II
PalmitoleoylCoA/PalmitoylCoA
p<0.0001
Ratio of relative levels
Control
SCD1-high
D
018z cells
CNS
BM
Spleen
p=0.0089
Number of blasts
CTL
SCD1 high
E
REH cells
CNS
BM
Spleen
p=0.0025
p=0.0282
Number of blasts
CTL
SCD1 high
F
INPUT
OUTPUT
Control: mCherry
Control: GFP+
BB : 45.75%
control : 49.96%
BB : 43.35%
control : 51.43%
Control: mCherry
SCD1-high: GFP+
SCD high : 51.00%
control : 48.33%
SCD high : 70.15%
control : 25.43%
G
p=0.0261
p=0.0386
Enrichment of SCD1-high blasts
CNS
BM
Spleen

FIGURE 3

Figure 3. *SCD1* overexpression confirms a competitive advantage for "SCD1-high" cells in the CNS microenvironment. (A) *SCD1* gene expression levels following *SCD1* overexpression in 018z cells. **(B)** Western blot of SCD1 protein after overexpression in 018z cells. **(C)I-II** Ratio of relative levels of oleoyl-CoA/stearoyl-CoA and of palmitoleoyl-CoA/palmitoyl-CoA in control (CTL) and SCD1-high 018z cells. p=Student's t-test. **(D)** Human leukemia burden in 018z xenograft model. Total amount of leukemic cells in CNS, BM and spleen of NSG mice xenografted with human 018z ALL cell line overexpressing *SCD1* (SCD1-high) or control (CTL) GFP^+ at the time of sacrifice. **(E)** Human leukemia burden in REH xenograft model. Total amount of leukemic cells in CNS, BM and spleen of NSG mice xenografted with human REH ALL cell lines overexpressing *SCD1* (SCD1-high) or control (CTL) GFP^+ at the time of sacrifice. p=paired Student's t-test. **(F)** Competition assay *in vivo***:** FACS plots of cells injected (INPUT) and cells isolated from the CNS of the mice at sacrifice (OUTPUT). Top: GFP^+ control cells transduced with a GFP-carrying lentiviral backbone and $mCherry^+$ control cells transduced with a mCherry carrying lentiviral backbone injected in a ratio of 1:1. Bottom: GFP+ *SCD1* overexpressing (SCD1-high) cells and $mCherry^+$ control cells transduced with a mCherry carrying lentiviral backbone injected in a ratio of 1:1. **(G)** Ratio of total number of SCD1-high 018z cells (GFP^+) to control 018z cells ($mCherry^+$) in CNS, BM and spleen of NSG mice transplanted with a mixture of the two cell types in a ratio of 1:1. The backbone vector for SCD1 overexpression was used as control vector. p=paired Student's t-test.

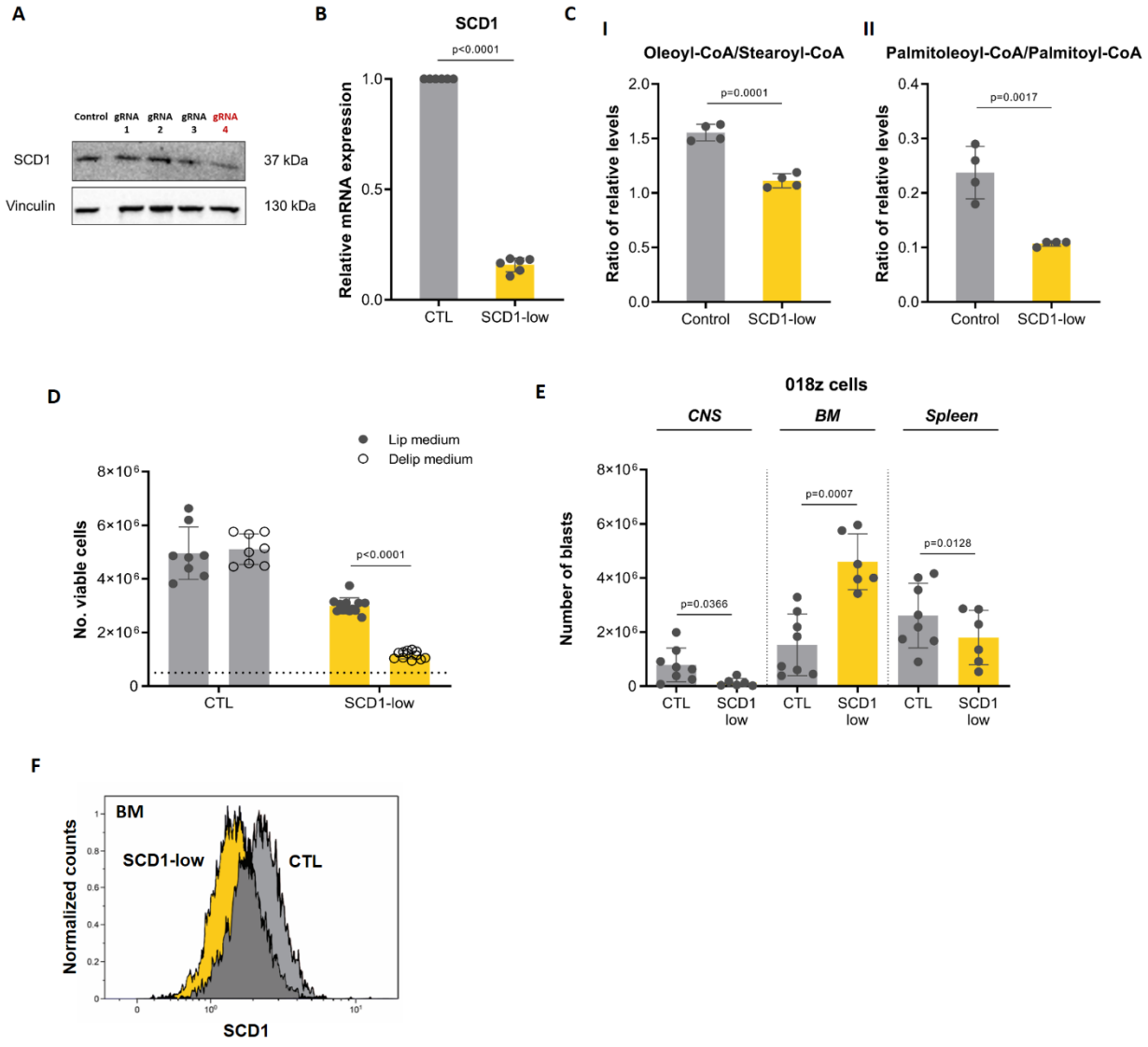

943

944

945

946

947

948

949 **FIGURE 4**

Figure 4. *SCD1* ablation decreases 018z cells engraftment in the CNS. (A) Western blot analysis of SCD1 after CRISPR-Cas9 gene ablation in 018z cells. Each lane represents a different gRNA used for the initial screening. gRNA4 decreased SCD1 protein expression while gRNA1-3 did not affect its levels. **(B)** Gene expression level of *SCD1* after CRISPR-Cas9 knockout in 018z cells by gRNA4. **(C)I-II** Ratio of relative levels of oleoyl-CoA/stearoyl-CoA and of palmitoleoyl-CoA/palmitoyl-CoA in control (CTL) and SCD1-low 018z cells. p=Student's t-test **(D)** *In vitro* proliferation of SCD1-low and control (CTL) 018z cells after 96 hours in in medium supplemented with 10% lipidated or delipidated FBS. The dotted line represents the initial number of cells plated at T0. p=two-way ANOVA. **(E)** Human leukemia burden in 018z xenograft model. Total amount of leukemic cells in CNS, BM and spleen of NSG mice xenografted with human 018z ALL cell lines SCD1-low or control GFP at the time of sacrifice. p=paired Student's t-test. **(F)** Intracellular staining of SCD1 in human cells isolated from the BM of mice transplanted with SCD1-low and control (CTL) 018z cells. The scramble vector for SCD1 downregulation was used as control vector. The peaks are relative to the percentage of human $CD19^+$ cells normalized to mode.

967

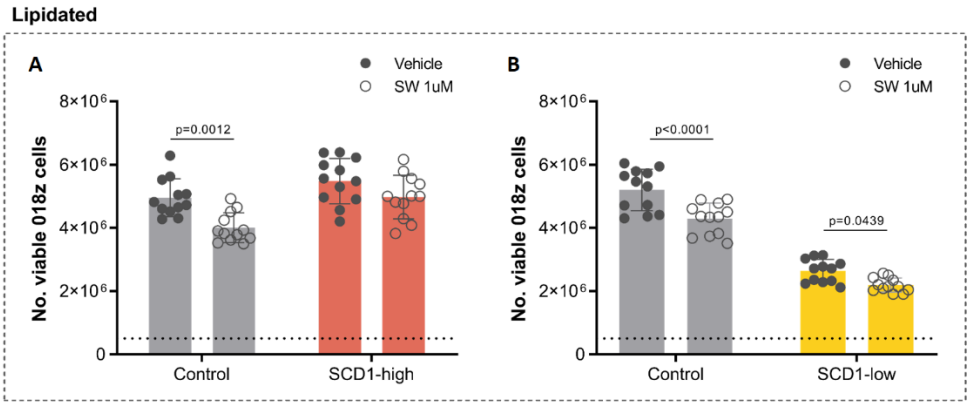
Lipidated
A
Vehicle
SW 1uM
No. viable 018z cells
8×10⁶
6×10⁶
4×10⁶
2×10⁶
0
p=0.0012
Control
SCD1-high
B
Vehicle
SW 1uM
No. viable 018z cells
p<0.0001
p=0.0439
Control
SCD1-low

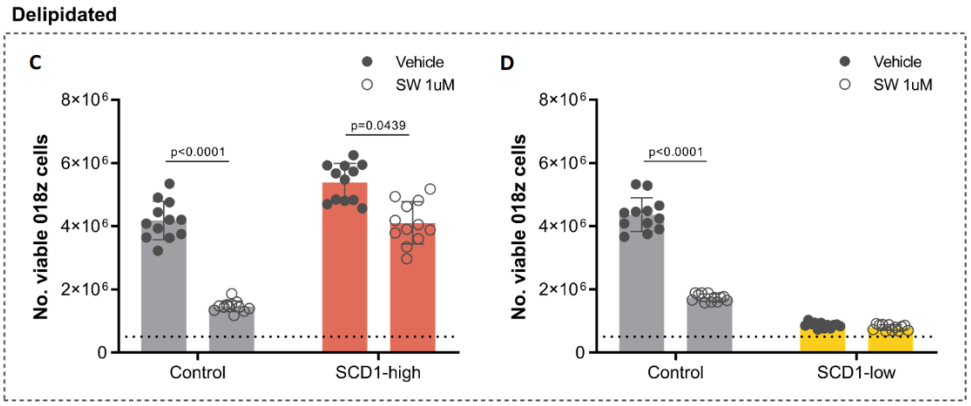
Delipidated
C
Vehicle
SW 1uM
No. viable 018z cells
p<0.0001
p=0.0439
Control
SCD1-high
D
Vehicle
SW 1uM
No. viable 018z cells
p<0.0001
Control
SCD1-low

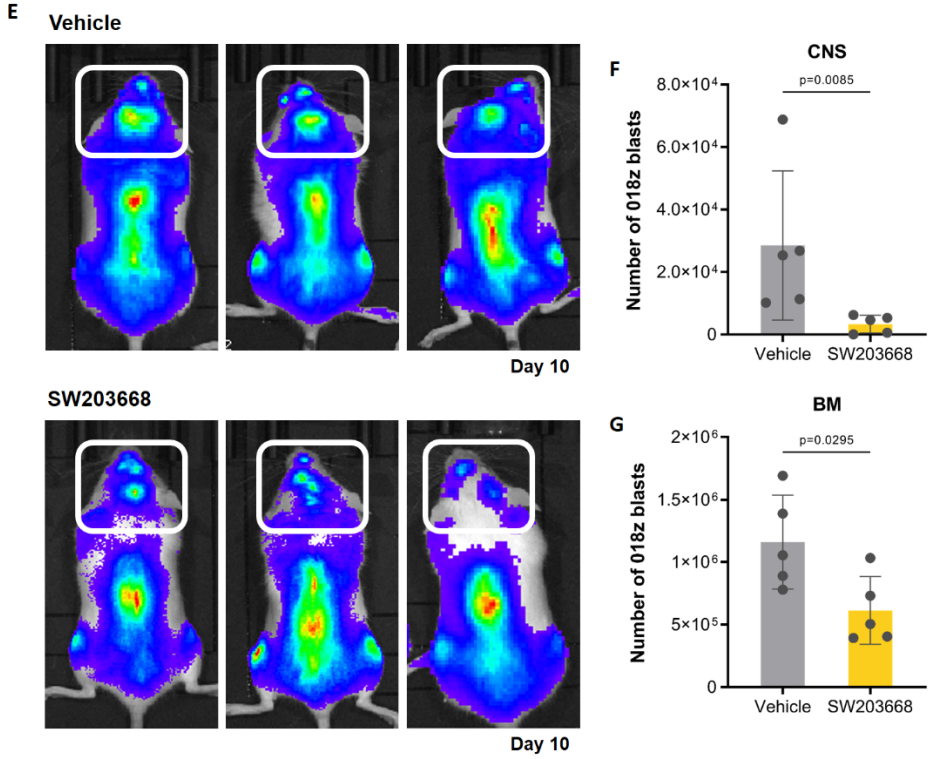
E
Vehicle
Day 10
SW203668
Day 10
F
CNS
p=0.0085
Number of 018z blasts
8.0×10⁴
6.0×10⁴
4.0×10⁴
2.0×10⁴
0
Vehicle
SW203668
G
BM
p=0.0295
Number of 018z blasts
2×10⁶
1.5×10⁶
1×10⁶
5×10⁵
0
Vehicle
SW203668

968

FIGURE 5

Figure 5. SCD1 pharmacological inhibition decreases 018z cells engraftment in the CNS. *In vitro* proliferation of "SCD1-high", "SCD1-low" and matching control (CTL) 018z cells after seeding $0.5x10^6$ cells/well for 96 hours in medium supplemented with 10% lipidated **(A-B)** or delipidated **(C-D)** FBS treated with 1μM of the SCD1 inhibitor SW203668 or vehicle (DMSO).The dotted line represents the initial number of cells plated at T_0. p=two-way ANOVA. **(D)** $GFP^+mCherry^+FFLuc^+$ 018z cells were injected intravenously to NSG mice and treated from day 1 to day 10 with the SCD1 inhibitor SW203668 or vehicle (n=5 group). Representative bioluminescence of the tumor load at the time of sacrifice in three different pairs of mice, top: vehicle treated mice; bottom: drug treated mice. Decrease in the tumor load is clear in the spine and the skull area (CNS – marked with white box). Total amount of leukemic cells in CNS **(E)** and BM **(F)** of NSG mice xenografted with human $GFP^+mCherry^+FFLuc^+$ 018z and treated with SW203668 for 10 days at the time of sacrifice. The backbone vector for SCD1 overexpression was used as control vector for SCD1-high and the scramble vector was used as control for SCD1-low. BM – bone marrow. p=Student's t-test.

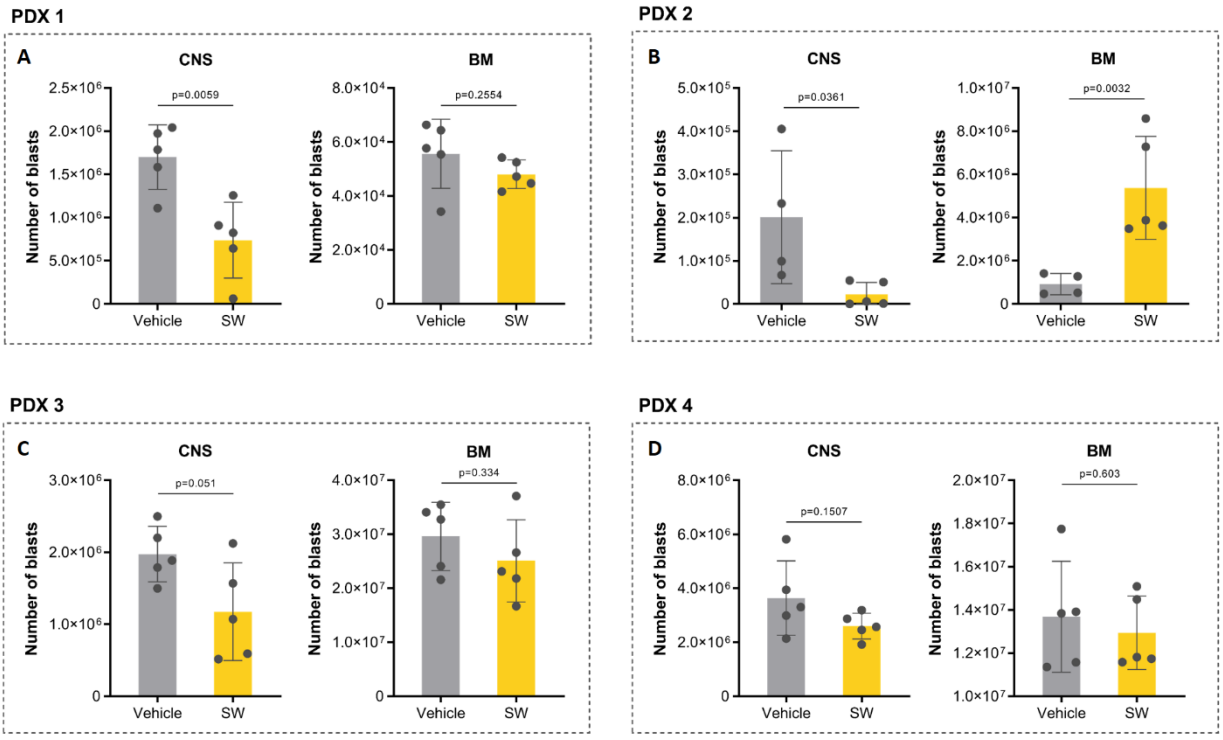
PDX 1
A
CNS
BM
Number of blasts
p=0.0059
p=0.2554
Vehicle
SW
PDX 2
B
p=0.0361
p=0.0032
PDX 3
C
p=0.051
p=0.334
PDX 4
D
p=0.1507
p=0.603

Figure 6. SCD1 pharmacological inhibition decreases patient-derived xenograft (PDXs) engraftment in the CNS. Human leukemia burden in PDXs. Cells from 4 different PDXs were injected intravenously into NSG mice. Xenografted mice were treated daily from day 7 with the SCD1 inhibitor SW203668 or vehicle (n=5 group) at 20 mg/kg. The total amounts of leukemic cells in CNS and BM of NSG mice at the time of sacrifice are plotted in the graphs **(A-D)**. p=Student's t-test.

Table 1. Precursors for *de novo* fatty acid synthesis in mice.

Metabolite	CSF:Plasma ratio (control)	CSF:Plasma ratio (leukemia)
Glucose	0.22 (0.13 – 0.33)	0.24 (0.16 – 0.46)
Glutamine	0.88 (0.62 – 1.08)	0.90 (0.62 – 1.38)
Lactate	0.19 (0.11 – 0.28)	0.19 (0.12 – 0.23)
Alanine	0.20 (0.14 – 0.24)	0.18 (0.10 – 0.26)
Pyruvate	0.87 (0.63 – 1.59)	1.05 (0.59 – 2.92)

Table 1. LC-MS quantification of key nutrients extracted from CSF and plasma of healthy (Control, n=8) and NSG mice and mice transplanted with the SEM cell line at clinical endpoint (n=6).